

Strain localization and fluid pathways in mylonite: inferences from in situ deformation of a water-bearing quartz analogue (norcamphor)

P. Bauer, S. Palm, M.R. Handy *

Institut für Geowissenschaften, Justus-Liebig Universität Giessen, Senckenbergstrasse 3, D-35390 Giessen, Germany

Received 15 March 1999; accepted for publication 31 January 2000

Abstract

Simple shearing of polycrystalline norcamphor containing 10–15 vol% water, at near-atmospheric pore fluid pressure and a range of constant temperatures (3–35°C) and shear strain rates (5×10^{-5} – $4 \times 10^{-4} \text{ s}^{-1}$), induces localization of both strain and fluid flow. Prior to deformation, the water is located at grain triple junctions and pockets along grain boundaries. It forms an average dihedral angle of 46° with the surrounding norcamphor grains. During initial shearing ($\gamma \leq 1$), grain boundaries oriented subparallel to the principal shortening direction dilate and fill with water. At $1 < \gamma < 2$, these open grain boundaries interconnect to form water-filled dilatant shear surfaces at low angles (10 – 15°) to the shear zone boundary. These surfaces resemble shear bands or C' surfaces in mylonitic rock and, depending on the temperature, accommodate displacement by cataclasis ($T < 15^\circ\text{C}$) or dislocation creep ($T > 15^\circ\text{C}$). The tips of the shear surfaces propagate alternately by intracrystalline plasticity and subcritical fracturing, concomitant with dynamic recrystallization in the rest of the sample. The episodic interconnection of dilatant shear surfaces is associated with short-term increases in displacement rate parallel to the surfaces. These surfaces coalesce to form a high-strain, fluid-filled network subparallel to the experimental shear zone. However, this network never spans the entire length of the shear zone at any given time, even after shearing to $\gamma = 8.5$. The deformation is more homogeneous and fewer dilatant shear surfaces develop at higher deformational temperatures and/or lower strain rates due to the increased activity of dislocation creep. Prolonged stress annealing removes most microstructural evidence of the syntectonic fluid pathways.

Dilatant shear surfaces in norcamphor resemble relics of mica-filled, synmylonitic fractures in dynamically recrystallized quartz from greenschist facies mylonite, suggesting that fluid played a similar mechanical role in nature and experiment. The coalescence of dilatant, fluid-filled shear surfaces represents a strain-dependent increase in pore connectivity within mylonitic shear zones. The experiments indicate that fluid flow along deep crustal mylonitic shear zones is probably limited by the rate at which the tips of the dilatant shear surfaces propagate subparallel to the shearing plane. © 2000 Elsevier Science B.V. All rights reserved.

Keywords: brittle–viscous transition; fluid pathways; mylonite; shear zone; strain localization; quartz analogue

* Corresponding author. Present address: FB-Geowissenschaften, Freie Universität Berlin, D-12249 Germany. Tel.: +49-30-7792-292.

E-mail address: mark.handy@geolo.uni-giessen.de (M.R. Handy)

1. Introduction

Shear zones are structural and mechanical heterogeneities that accommodate localized deformation on different scales (e.g. Dutrege and Burg, 1998). Thus, shear zones regarded on the regional and outcrop scales are the geometric and kinematic equivalents of microshears or shear surfaces on the microscopic and hand-specimen scales. Shear zones nucleate and grow in several orientations, depending on the kinematics of shearing, the shape of the strain ellipsoid (Gapais et al., 1987), and the amount of strain (Herwegh and Handy, 1998). These orientations, depicted in Fig. 1 for simple shearing, are independent of the material and are similar for cataclastic fault rocks and mylonitic rocks (Shimamoto, 1989). We therefore use the term ‘shear surface’ to refer generally to shear fractures (R surfaces) or shear bands (C' surfaces) oriented at low angles ($<45^\circ$) to the main foliation (P, S surfaces) and bulk shear plane (Y, C surfaces). Following Schmid and Handy (1991), we consider material that undergoes microcracking, frictional sliding, and rigid body rotation to be a cataclasite or cataclastic, whereas material in which the matrix deforms by one or more thermally activated creep mechanisms (dislocation glide, dis-

location climb, diffusion-accommodated grain boundary sliding, pressure solution) is described as a mylonite or as mylonitic.

Mineralogical, geochemical and isotopic studies have documented the importance of shear zones as advective pathways for metamorphic fluids (McCaig et al., 1990; Newton, 1990; Selverstone et al., 1991), yet the mechanisms of fluid migration are poorly understood. Such studies indicate that fluids flow both upwards (McCaig et al., 1990; Fricke et al., 1992) and downwards (Etheridge et al., 1988) within shear zones, apparently irrespective of the shear zone kinematics. Lithostatic pressure tends to drive fluid upwards (i.e. down the lithostatic pressure gradient) towards the Earth’s surface, but either upward or downward fluid migration can arise from local fluid pressure gradients associated with the episodic opening and closing of cracks (‘seismic pumping’ of Sibson et al., 1975; Etheridge et al., 1984). The relationship between fluid migration, fracture propagation and mylonitization in deep crustal shear zones remains unclear. In part, this reflects the multiple mechanical roles of metamorphic fluid. On the one hand, fluid can weaken rock because it induces pressure solution at grain boundaries (Rutter, 1983), enhances intracrystalline dislocation mobility (Jaoul et al., 1984), and can trigger hydrofracturing by exerting pore pressure (Handin et al., 1963; Murrell, 1965). On the other hand, fluid can strengthen rock by serving as a diffusive medium for the precipitation of minerals that seal cracks and veins (Blanpied et al., 1992). Increased strength also results from reduced effective pressures during transient fluid flow out of rocks during brittle, dilatant deformation (‘dilatancy hardening’; Rutter, 1972).

Although various experimental approaches have been employed to examine the role of fluid during deformation (undrained and drained triaxial experiments on rocks), most studies have focused on rheological effects of increased pore fluid pressure during syntectonic dehydration reaction (Raleigh and Paterson, 1965; Heard and Rubey, 1966), or of the growth of very fine-grained reaction products (Brodie and Rutter, 1987). Zhang et al. (1994) measured strain-dependent changes in permeability of experimentally

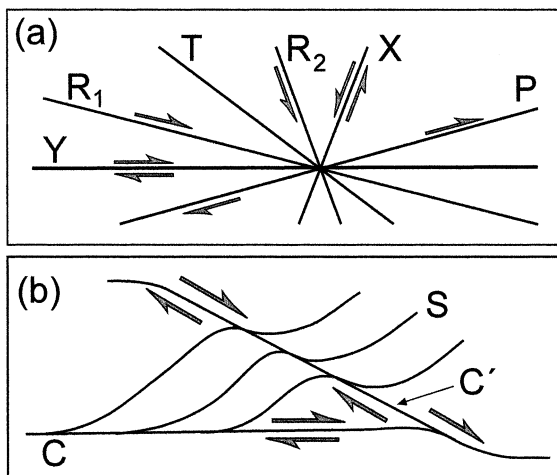


Fig. 1. Planar structures generated during simple shearing: (a) planes in cataclastic fault rocks (modified after Logan et al., 1992; Petit, 1987); (b) planes in mylonitic rocks (modified after Platt and Vissers, 1980; Gapais et al., 1987).

deformed marble, but as in all high-pressure experiments, the samples were deformed in sealed vessels, precluding direct observation of the evolving microstructures, deformation mechanisms and fluid pathways during deformation. Urai (1983) deformed salt rocks under the optical microscope to investigate changes in fluid distribution along grain boundaries during syntectonic grain boundary migration. However, studies of naturally deformed rocks indicate that, in addition to grain scale processes, strain partitioning on the supragranular scale controls advective fluid flow associated with syntectonic metamorphism (e.g. Brodie and Rutter, 1985; Bell and Hayward, 1991).

In this paper, we report a series of deformation experiments on polycrystalline norcamphor, a quartz analogue material, that were designed to characterize the relationship between strain localization and fluid migration in crustal rocks undergoing mylonitic deformation at constantly high pore fluid pressures. Following an approach pioneered by Means (1977, 1989) and Urai et al. (1980), we conducted these experiments *in situ*, i.e. in transmitted, polarized light with an optical microscope, in order to monitor the evolving microstructure of a rock analogue during deformation. This approach has been successfully employed under dry (non-aqueous) conditions to simulate microfabric evolution in quartz (e.g. Means, 1989; Herwegh et al., 1997), but its use here to investigate syntectonic fluid migration on scales exceeding that of individual grains is unprecedented. The next section therefore contains a detailed description of the experimental conditions, sample preparation methods and materials. In subsequent sections, we present microstructural evidence supporting the notion that strain localization and focusing of fluid flow are intimately related processes. In particular, we found that structures form whose orientation is related both to the high pore fluid pressure and to the kinematics of deformation. These experimental structures are then compared with the geometry of relict fluid pathways in dynamically recrystallized quartz. Based on these results, we consider how deformation effects change in the connective porosity and permeability of mylonite.

2. Experimental techniques, sample properties and preparation

2.1. Experimental techniques

The modified Urai–Means apparatus used to deform and view the norcamphor rock analogue under a polarizing optical microscope (pictured in Fig. 2a) has been described by Bauer et al. (1999). It includes a synchronous motor connected by a flexible coupling to a spindle drive that moves a ram into a deformation cell. This ram displaces a glass plate with a frosted strip, which in turn adheres to and therefore deforms the norcamphor sample above a lower glass plate that remains stationary within the cell (inset, Fig. 2a). Polarized light passes through the window in the deformation cell containing the glass plates and sample. Friction between the sample and the glass plates is minimized by coating the plates with silicon oil. The procedures used to analyse the microstructure during deformation are described in detail by Herwegh and Handy (1998) and Bauer et al. (1999).

2.2. Materials and sample preparation

We used polycrystalline norcamphor (C_7H_9OH) mixed with small amounts (~ 10 vol%) of distilled water to simulate the grain scale effects of fluid on deforming quartz microstructure. Bons (1993) was the first to adopt norcamphor as a rock analogue. It is hexagonal, optically uniaxial negative, and has a birefringence of 0.005 to 0.01. When deformed as a dry aggregate (i.e. in the absence of water) at room temperature, norcamphor develops microstructures commonly observed in quartzite, that experienced dislocation creep at greenschist to amphibolite facies conditions (Herwegh and Handy, 1996). The addition of approximately 10 vol% water to norcamphor lowers its melting point from about 96°C at dry conditions to approximately 55°C.

The following preparation procedure yielded norcamphor samples with an equigranular, foam-like microstructure containing fluid within intergranular pockets and triple junctions (Fig. 2b). Norcamphor powder (initial grain size 50 μm) is

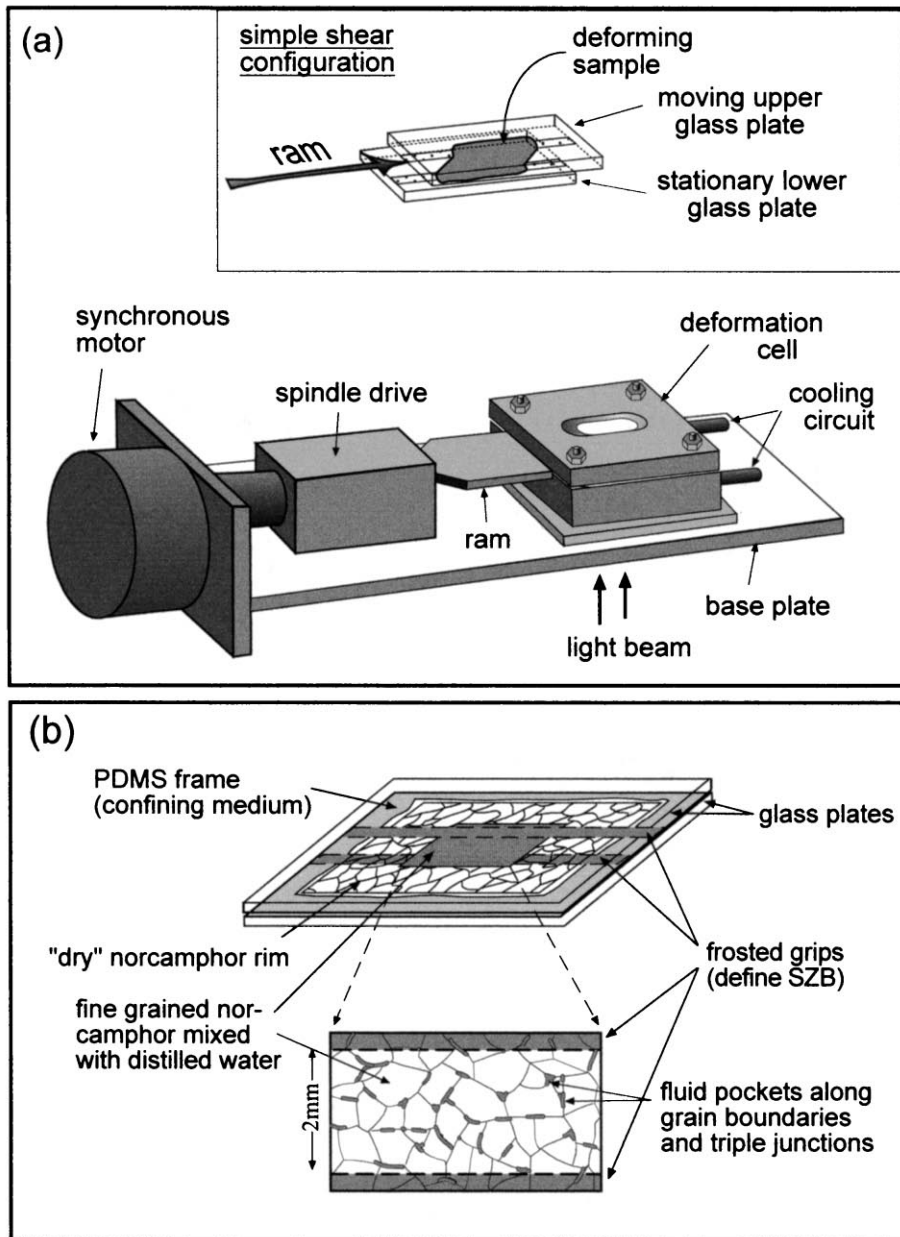


Fig. 2. Experimental configuration: (a) Urai-Means deformation rig for in situ experiments; (b) sample of norcamphor with water prior to deformation.

mixed with corundum particles (grain size 9 μm , grid 600) that serve as passive markers for strain analysis (method of Bons et al., 1993). This material is then cold pressed in a die with a hand-driven hydraulic press (load=2 metric tons) to a

disc shape (diameter=30 mm) with a thickness of about 500 μm , and then placed on one of the glass plates. A rectangular piece is cut out of the centre with a razor blade, leaving a frame of dry norcamphor. The rectangular piece (approximately

$10 \times 2 \text{ mm}^2$) is fragmented and the pieces re-inserted in the frame to ensure a homogeneous distribution of marker particles within the sample area. Distilled water is then added to the fragments within the frame. The dry norcamphor frame confines the norcamphor fluid aggregate. The sample and its dry rim are then framed with a polymer substance (polydimethyl-siloxane, abbreviated PDMS; Weijermars, 1986) and covered with the upper glass plate. This procedure prevents sublimation of norcamphor and loss of fluid during deformation. After placing the glass plates containing the prepared sample in the deformation cell, the temperature is raised to 45°C without tightening the four screws on the metal covering plate (Fig. 2a). This enables dendritic crystals to precipitate on the upper glass plate. Their coalescence results in an equilibrium, foam-like microstructure. Tightening the screws for 4 to 7 days hot presses the sample coaxially to a thickness of about 150 to 200 μm . This thickness is about equal to the final average grain diameter (100 and 200 μm).

The sample therefore consists of at least one layer of equigranular norcamphor grains.

2.3. Properties of norcamphor with water

The grain boundaries in the water-bearing norcamphor samples are less regular than in dry samples, probably because fluid pockets at grain boundaries inhibit grain boundary migration during hot pressing. The dihedral angle of norcamphor/norcamphor/water interfaces is about 46° and therefore well within the range of dihedral angles ($\leq 60^\circ$) required for grain edge fluid channels to form in an isotropic grain aggregate (Holness, 1997 and references cited therein). This dihedral angle would enable fluid to flow within narrow tubules and bubbles along norcamphor grain boundaries if differences in fluid pressure existed within the sample or between the sample and its surroundings.

The solubility of norcamphor in water at different temperatures was determined at atmo-

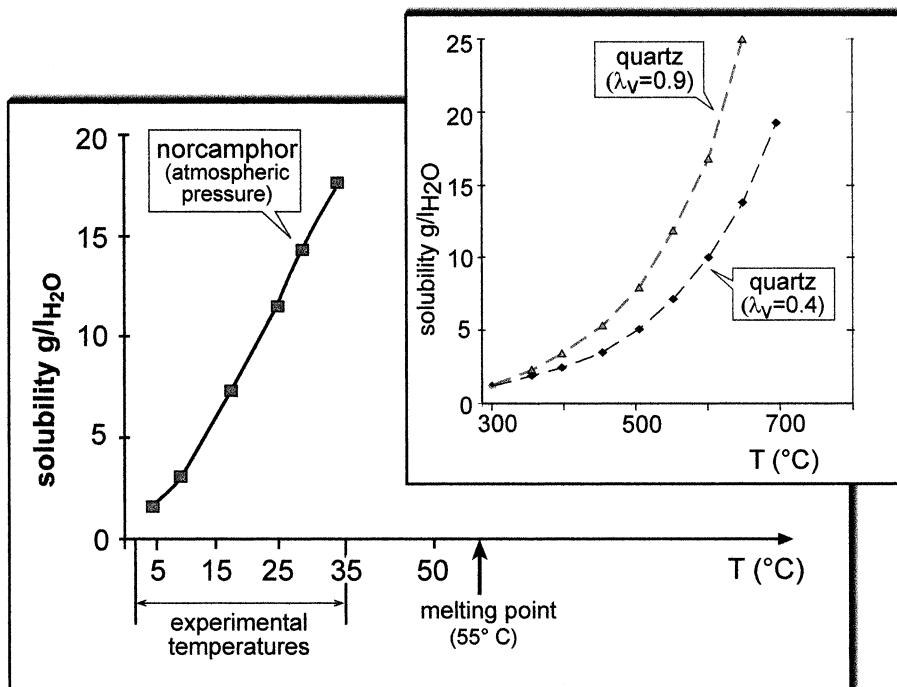


Fig. 3. Solubilities of norcamphor and quartz in water as a function of temperature. Quartz solubilities at $\lambda_v = 0.4$ and 0.9 after Streit and Cox (1998) along a geobar of 26.5 MPa/km. Norcamphor solubility measured at atmospheric pressure.

spheric pressure to help assess the potential role of pressure solution in the experiments and to compare this with quartz solubilities. Fig. 3 shows that norcamphor is obviously much more soluble in water than quartz. The amount of dissolved norcamphor in distilled water at room temperature and pressure is comparable with that of quartz in water at 600°C and hydrostatic pressure (pore fluid factor $\lambda_v=0.4$, where λ_v =ratio of pore fluid pressure to lithostatic pressure, P_f/P_l) along a geobar of 26.5 MPa/km (quartz solubilities after Streit and Cox, 1998). Elevated pressures (i.e. higher pore fluid factors) significantly increase the solubility of quartz in water. Of course, pressure solution in any crystalline material is also affected by the kinetics of diffusional transport, as well as the rates of dissolution and precipitation in an anisotropic stress field. Unfortunately, no solubility data are available for stressed norcamphor at applied confining pressure. The activity of pressure solution with respect to other deformation mechanisms in norcamphor is discussed in the sections below.

After the norcamphor samples were annealed, no air pockets remained in the aggregate, and there was no evidence for any leakage of fluid or volume change of the sample. Thus, the average pore fluid pressure in the sample was probably about equal to the atmospheric confining pressure (i.e. $\lambda_v \approx 1$). With the sample preparation method and configuration described above, the average pore fluid pressure within the norcamphor fluid aggregate remained at this level throughout the experiment. Near-lithostatic pore fluid pressures appear to be common in quartz-rich rocks deforming by dislocation creep under greenschist to amphibolite facies conditions (e.g. Etheridge et al., 1983; Streit and Cox, 1998). Our experiments therefore simulate high-temperature mylonitization of a fluid-bearing quartzite at near-lithostatic pore fluid pressures below the seismogenic regime.

2.4. Analytical methods

Several methods were used to record and analyse the microstructural evolution. Microstructural changes during the experiment were documented with time-lapse videos, colour slides and black-

and-white photographs. These images were then analysed with the computer program NIH Image to estimate the fluid content, to determine the orientation, dimensions and distribution of fluid-filled surfaces, and to measure rates of surface tip propagation and grain boundary migration. Strain analysis involved digitizing the positions of the corundum marker particles on black-and-white photos and digitized time-lapse videos with NIH Image, and then using the program Marker Analysis (Bons et al., 1993) to calculate incremental strain grids from changes in the relative positions of these particles during the experiment. Strain is visualized as contour plots of axial ratios of the finite strain ellipsoid, as calculated at every node of the incremental strain grid.

The choice of the size (9 mm) and density of the corundum marker particles in our experiments is governed by the desire to maximize particle resolution on several different scales of observation without affecting the sample microstructure. There is a trade-off between particle size and density: a large number of small particles could not have been resolved at the largest scales of observation and would have pinned mobile grain boundaries, thereby hindering the microstructural evolution. On the other hand, a small number of large particles would obviously reduce our ability to quantify strain in the sample, especially at very small scales. We opted for the same particle size and approximately the same particle density in all experiments in order to be able to compare strain distribution and microstructural evolution on several different scales between individual experiments. The reader is referred to Herwegh and Handy (1996, 1998) for a detailed description of the strain analysis procedure employed in this study.

The fluid in the samples was most easily recognized in plane light as areas of high optical relief, particularly adjacent to boundaries with norcamphor grains. Fluid appears as dark grey to black regions in the black-and-white photomicrographs of this paper. Where the intergranular fluid films were particularly thin, we could only determine the nature and configuration of the grain-grain and grain-fluid contacts by 'focusing through' the sample, i.e. by raising and lowering

the microscope objective with respect to the sample. Due to the thickness of the samples and the complex nature of the grain–grain and grain–fluid contacts, it is impossible to provide sharp photographic images of all the microstructures at a given focal depth within a given sample, especially at higher magnifications. We therefore supplemented a number of the photographs below with line drawings.

3. Evolution of microstructures and fluid pathways

3.1. General

Simple shearing of water-bearing ('wet') polycrystalline norcamphor was carried out at temperatures ranging from 3 to 35°C (0.05 to $0.65 T/T_{\text{melting}}$) and shear strain rates of $\dot{\gamma} = 10^{-4}$ to 10^{-5} s^{-1} . The conditions of each experiment are indicated in Fig. 4. In all experiments, norcamphor deformed primarily by a combination of localized fracturing and intracrystalline plasticity. At the

same conditions, dry norcamphor deforms predominantly by dislocation creep and shows no brittle deformation. Dry samples are characterized by rapid grain boundary migration recrystallization, the development of strong shape and crystallographic preferred orientations (SPO, CPO) of dynamically recrystallized grains, and the nucleation and growth of mylonitic microshear zones (Herwegh and Handy, 1996, 1998). Intergranular fracturing was only observed in dry samples that were deformed at a temperature of 4°C and a shear strain rate of $5.5 \times 10^{-4} \text{ s}^{-1}$ (Herwegh et al., 1997). The presence of a grain boundary fluid at lithostatic or near-lithostatic pressure therefore enhances brittle behaviour during mylonitic deformation. This enhancement is directly related to strain-dependent changes in the distribution of fluid, as described below.

The fluid occupied two different sites during our experiments (Fig. 5a): (1) intergranular pockets, films and channels between the two glass slides; (2) discs along the interface of the norcamphor grains and glass slides. Whereas intergranular fluid was redistributed during deformation, the fluid discs between the sample and the glass slides remained stationary with respect to the latter for the duration of the experiment. In fact, some fluid discs behaved as passive strain markers, becoming more elliptical with progressive simple shearing (Fig. 5b–d). No fluid was observed to migrate along the sample–glass interface during the experiment. Therefore, only fluid occupying the sites in (1) above is relevant in this study.

3.2. Initial shearing and fluid redistribution

During initial shearing ($\dot{\gamma} < 1$), norcamphor grains deformed primarily by a combination of intracrystalline plasticity and pressure solution. Dislocation glide-plus-creep is evident from widespread undulose extinction, deformation bands and subgrains, whereas pressure solution was more difficult to establish given the low density of corundum strain markers at the small scales of observation. In Fig. 5b–d, syntectonic solution and precipitation of norcamphor is indicated by the movement of grain–fluid contacts with respect to corundum marker particles. For example, the

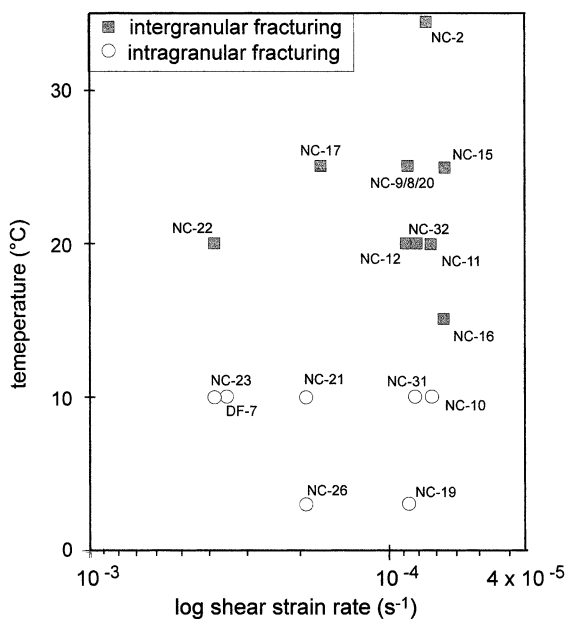
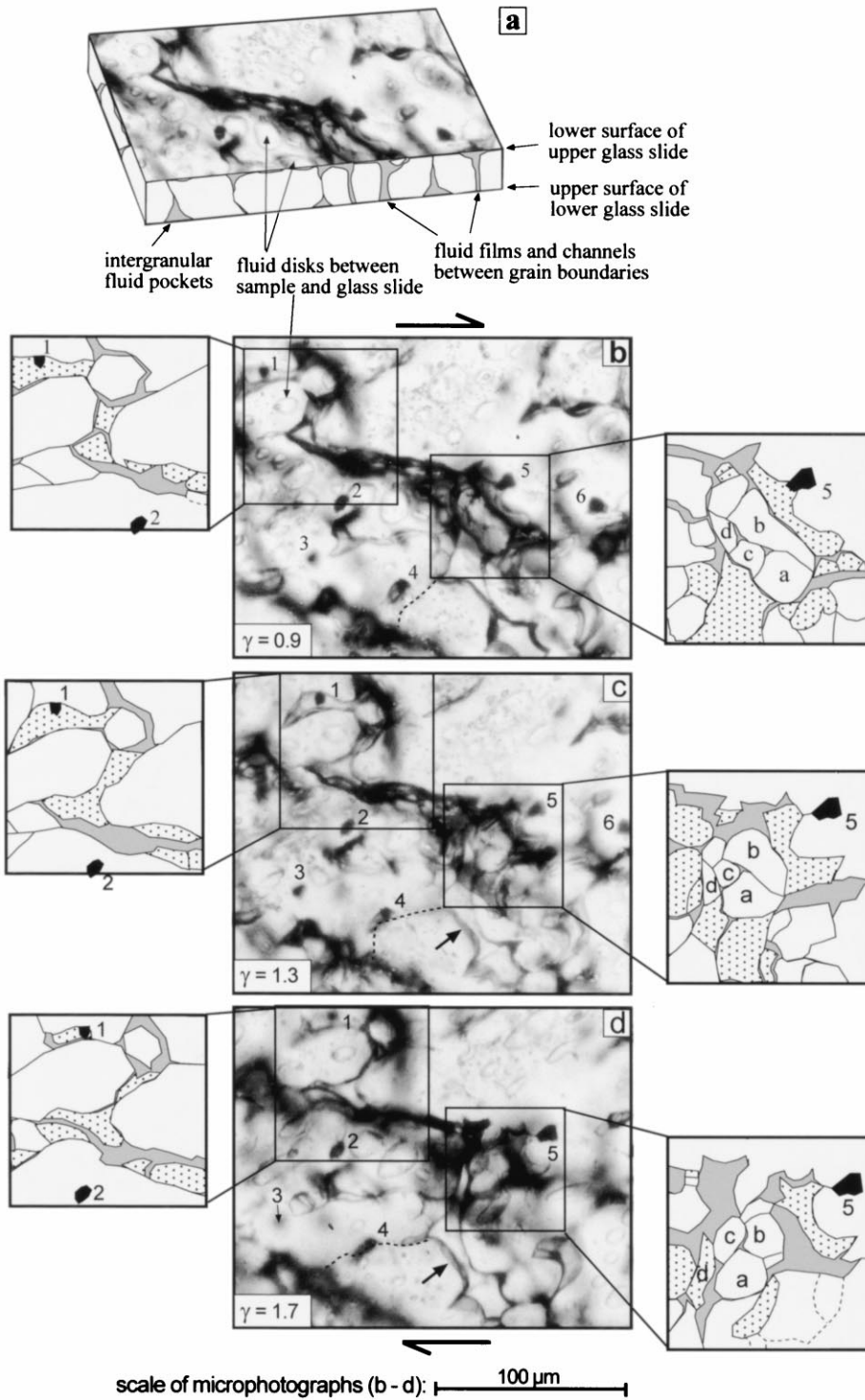


Fig. 4. Temperature–strain rate conditions of simple shearing in this study. Numbers refer to individual experiments. Squares and circles refer to type of fracturing at the propagating tips of dilatant shear surfaces (see text).



decrease in area of the norcamphor aggregate containing grains labelled a to d (right-hand insets) is diagnostic of localized dissolution. This grain aggregate is probably stressed, as it bridges the gap between the norcamphor walls. In contrast, the movement of the grain–fluid contacts nearest to marker particles 1 to 4 indicates localized precipitation and grain growth into fluid-filled voids. The grain–fluid contact to the right of particle 4 is curvilinear and locally faceted, indicating grain growth in the direction of the thick arrow in Fig. 5c and d.

Grain boundary migration recrystallization was prevalent in the entire sample, although difficult to distinguish from pressure solution, even in the presence of appropriately located marker particles. In Fig. 5, for example, the boundaries between grains a to d (right-hand insets) are clearly mobile, but appear to contain fluid films at some stages of their evolution (Fig. 5b and c). This may indicate non-conservative grain boundary migration, in which grain boundary mobility is partly accommodated by dissolution and precipitation norcamphor along neighbouring grains (Urai et al., 1986; Ree, 1994). The dotted line just below marker particle 4 (Fig. 5b) represents a grain–grain boundary that does not appear to contain a fluid film and that migrates quickly with respect to the marker particle (Fig. 5b–d). In time-lapse videos of the evolving microstructure, we observed that wetted or fluid-filled grain boundaries migrate more slowly than those that are free of fluid.

Changes in the fluid distribution during initial deformation ($\gamma \leq 1$) are quite remarkable, as shown in Fig. 5. Fluid migrates from interstitial pockets along the norcamphor grain boundaries and grain triple junctions to dilating grain boundaries that are oriented subparallel to the principal shortening direction at 45° to the SZB. Fluid-filled pockets oriented at higher angles to this direction close, as

also observed by Drury and Urai (1990) in octachloropropane (OCP), another quartz analogue material. The cause of the fluid redistribution appears to be small, localized pore fluid pressure gradients within the sample during intracrystalline plastic deformation; the fluid is squeezed or sucked into and along the dilating grain boundaries.

With progressive strain in the interval $1 < \gamma < 2$, the dilating grain boundaries interconnect to form elongate, fluid-filled surfaces (Fig. 6). We refer to these new surfaces as dilatant shear surfaces because once they attain a length of 300 to 600 μm (about two to four times the average grain diameter), they accommodate large displacements parallel to their lengths. The formation of these shear surfaces and their interconnection involves a combination of dynamic recrystallization, pressure solution (above and Fig. 5) and intergranular fracturing (Fig. 7).

Regarded on the scale of the entire sample (Fig. 6), the orientation of most dilatant shear surfaces with respect to the SZB (10 to 20°) falls within the range of orientations expected for synthetic shear (R1) fractures in cataclasite or C' planes in mylonite (Figs. 1 and 6). Only surfaces near the margins of the sample (i.e. near the SZB) were oriented at lower angles to the SZB (5 to 10°), corresponding to boundary shear fractures (Y surfaces in Fig. 1) at the edge of cataclastic shear zones (Logan et al., 1992). A small number of shear fractures are oriented at high angles to the SZB, corresponding to antithetic (R2 and X) shear surfaces (Figs. 1 and 6).

By a shear strain of about $\gamma = 2$, previously formed dilatant shear surfaces lengthen without broadening (average width of 30 μm) and only accommodate displacement parallel to their length. At the same time, new shear surfaces continue to nucleate in the dynamically recrystallizing, fluid-bearing norcamphor matrix. The deformation

Fig. 5. Norcamphor fluid microstructures during the interconnection of pore space at low to moderate shear strains: (a) block diagram showing three-dimensional distribution of fluid in the sample and black-and-white microstructural images; (b–d) microstructural sequence showing fluid redistribution in norcamphor during simple shearing. Numbers refer to corundum marker particles, small letters indicate individual grains discussed in text. Insets to right and left are line drawings of mobile grain–grain and grain–fluid contacts (see text). White areas are grains in contact with the upper glass slide, stippled areas are grains in contact with the lower glass slide only and above which there is fluid, grey areas contain fluids only. Experimental conditions: $T = 10^\circ\text{C}$, $\dot{\gamma} = 1.9 \times 10^{-4} \text{ s}^{-1}$.

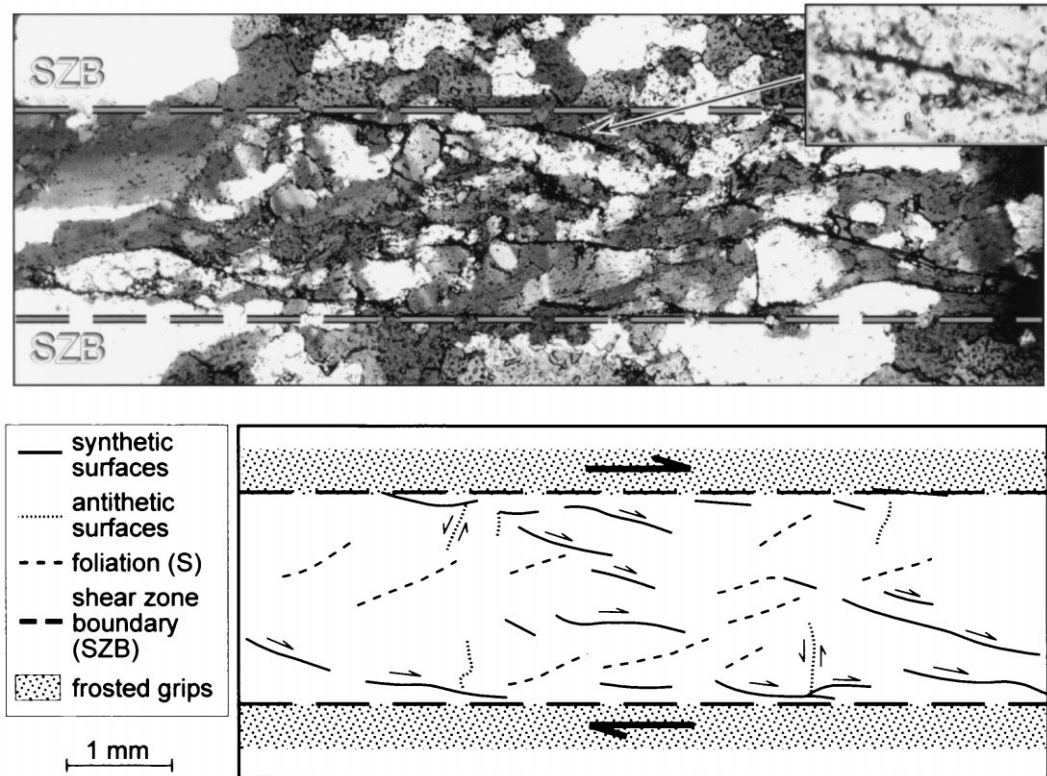


Fig. 6. Simple shearing experiment at $\gamma = 3.8$. (a) Photograph of sheared norcamphor sample taken with crossed nichols and inserted gypsum plate. Inset in upper left-hand corner contains grey-scale, plane light micrograph of a fluid-filled, dilatant shear surface. (b) Sketch of planar structures in (a). Solid lines = dilatant shear surfaces, dashed lines = foliation defined by long axes of dynamically recrystallizing norcamphor grains. Experimental conditions: $T = 10^\circ\text{C}$, $\dot{\gamma} = 8 \times 10^{-5} \text{ s}^{-1}$.

mechanisms that accommodate displacement parallel to the margins of the dilatant shear surfaces vary with temperature. At low temperatures ($T < 10\text{--}15^\circ\text{C}$), cataclasis is the dominant mechanism and reduces the size of grains which locally impinge along the irregular shear surfaces. At higher temperatures, grain size reduction at the margins of the dilatant shear surfaces involves pressure solution and progressive subgrain-rotation recrystallization. Irrespective of experimental temperature, the rest of the sample between the dilatant shear surfaces continues to undergo dynamic recrystallization. In these areas, grain boundary migration recrystallization is more active than subgrain-rotation recrystallization at temperatures greater than 20°C . The long axes of dynamically recrystallized grains define a shape-preferred orientation (SPO) that leans in the direction of

shear at $40\text{--}60^\circ$ to the SZB (S surfaces in Fig. 6). This SPO rotates synthetically with progressive strain, and after 20° rotation is replaced by a new SPO at 60° to the SZB, as described by Herwegh and Handy (1998) for dry, dynamically recrystallizing norcamphor.

3.3. Microstructures at intermediate to high shear strains

With continued shearing at $\gamma > 2$, dilatant shear surfaces lengthen and interconnect while the matrix undergoes grain boundary migration recrystallization. The tips of the dilatant shear surfaces propagate by a time- and strain-dependent combination of deformation mechanisms. As mentioned above, initial tip propagation (at shear strains of $\gamma < 2$) involves intergranular fracturing. At higher bulk

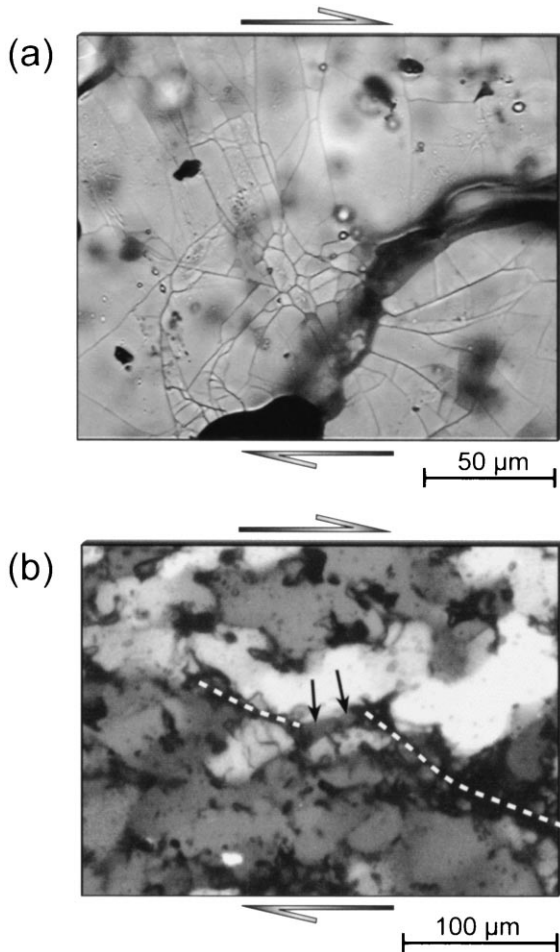


Fig. 7. Microstructures at the propagating tip of a dilatant shear surface: (a) intragranular fractures in norcamphor; (b) subgrains and dynamically recrystallized grains. Arrows point to newly nucleated subgrains between converging tips of dilatant shear surfaces. Experimental conditions: (a) $T=4^{\circ}\text{C}$, $\dot{\gamma}=2 \times 10^{-4} \text{ s}^{-1}$; (b) $T=20^{\circ}\text{C}$, $\dot{\gamma}=8.6 \times 10^{-5} \text{ s}^{-1}$.

shear strains, however, propagation occurs by both fracturing and intracrystalline plasticity (Fig. 7). The dominant fracture mechanism varies with temperature (squares and circles in Fig. 4). At temperatures greater than $10\text{--}15^{\circ}\text{C}$, intergranular fracturing predominates, whereas intragranular fracturing is favoured at lower temperatures (Fig. 7a). Both types of fracture propagate subcritically (maximum velocity $\sim 3 \times 10^{-6} \text{ m/s}$), as measured with time-lapse videos of the propagating

shear surfaces. Unfortunately, a strain-rate dependence of the fracture mechanisms could not be established due to the paucity of experiments at temperatures between 10 and 20°C and over the full range of experimental strain rates (Fig. 4).

The propagation of the shear surface tips by intracrystalline plasticity is much slower than by fracturing. Intracrystalline plasticity is marked by pronounced undulose extinction and subgrain-rotation recrystallization in the vicinity of the tips (arrows in Fig. 7b). The transition from tip propagation by intracrystalline plasticity to fracturing, and back again, is associated with strain and stress concentration at the converging tips of dilatant shear surfaces, as shown in Fig. 8. The domain between converging dilatant shear surfaces (Fig. 8a–c) coincides with a strain maximum in the centre of the strain contour plots (Fig. 8c and d). Displacement along the dilatant shear surfaces is initially accommodated by ductile deformation of the large, bright grain labelled A in the centre of Fig. 8a. This grain then breaks down along intragranular fractures that extend from the converging surfaces (Fig. 8b) and eventually interconnect (Fig. 8c). The subgrain size and dynamically recrystallized grain size in the tip regions between the two converging, dilatant shear surfaces are smaller than in the adjacent norcamphor matrix (Fig. 7b), indicating that the propagating tips are also the sites of pronounced stress concentration. Further displacement leads to fracturing of the dynamically recrystallized grains between the dilatant shear surfaces. The two surfaces then merge to form an even longer, high strain surface that extends across the field of view (Fig. 8c and e). Continued propagation of this composite surface involves renewed intracrystalline plasticity at its tips.

3.4. Interaction of dilatant shear surfaces

The growth and coalescence of dilatant shear surfaces is associated with fluctuating displacement rates parallel to these surfaces, as seen in Fig. 9. For example, the three-fold increase in the length of surface 1a going from Fig. 9a to b is associated with a nearly five-fold increase in the displacement

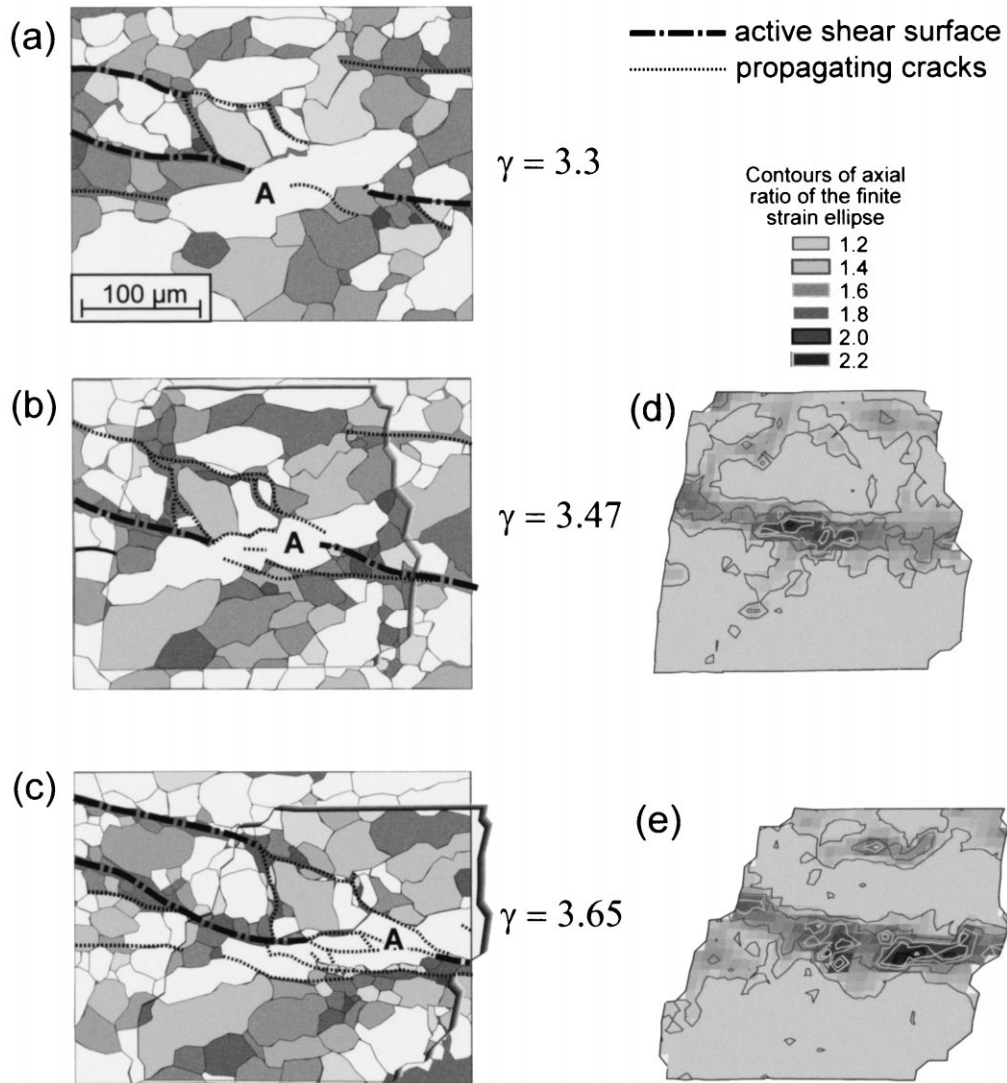


Fig. 8. Propagation and interconnection of tips of dilatant shear surfaces. (a–c) Grain boundary drawings showing propagation of surfaces and associated cracks with respect to the grain boundaries. Grey shades in the grains indicate the degree of optical extinction as observed with crossed polarizers. Grain labelled A is transected by fractures. (d, e) Contours of the axial ratios of the finite strain ellipse for the microstructure outlined, respectively, in (b) and (c). See text for explanation. Experimental conditions: $T=10^{\circ}\text{C}$, $\dot{\gamma}=1.9 \times 10^{-4} \text{ s}^{-1}$.

rate along this surface (Fig. 9e). Just before the coalescence of surfaces 1a and 1b (Fig. 9c), the displacement rate decreases (Fig. 9e). Once these two surfaces have interconnected, the displacement rate increases again (Fig. 9d and e). A similar evolution is documented in Fig. 9 for surface 2 near the SZB. Detailed measurements of evolving

surfaces as recorded in time-lapse videos indicate that for a given dilatant shear surface, intervals of increasing displacement rate correspond to tip propagation by fracturing and fracture coalescence, in the manner described above and shown in Fig. 8. Displacement rates decrease when the dilatant shear surfaces propagate more slowly by

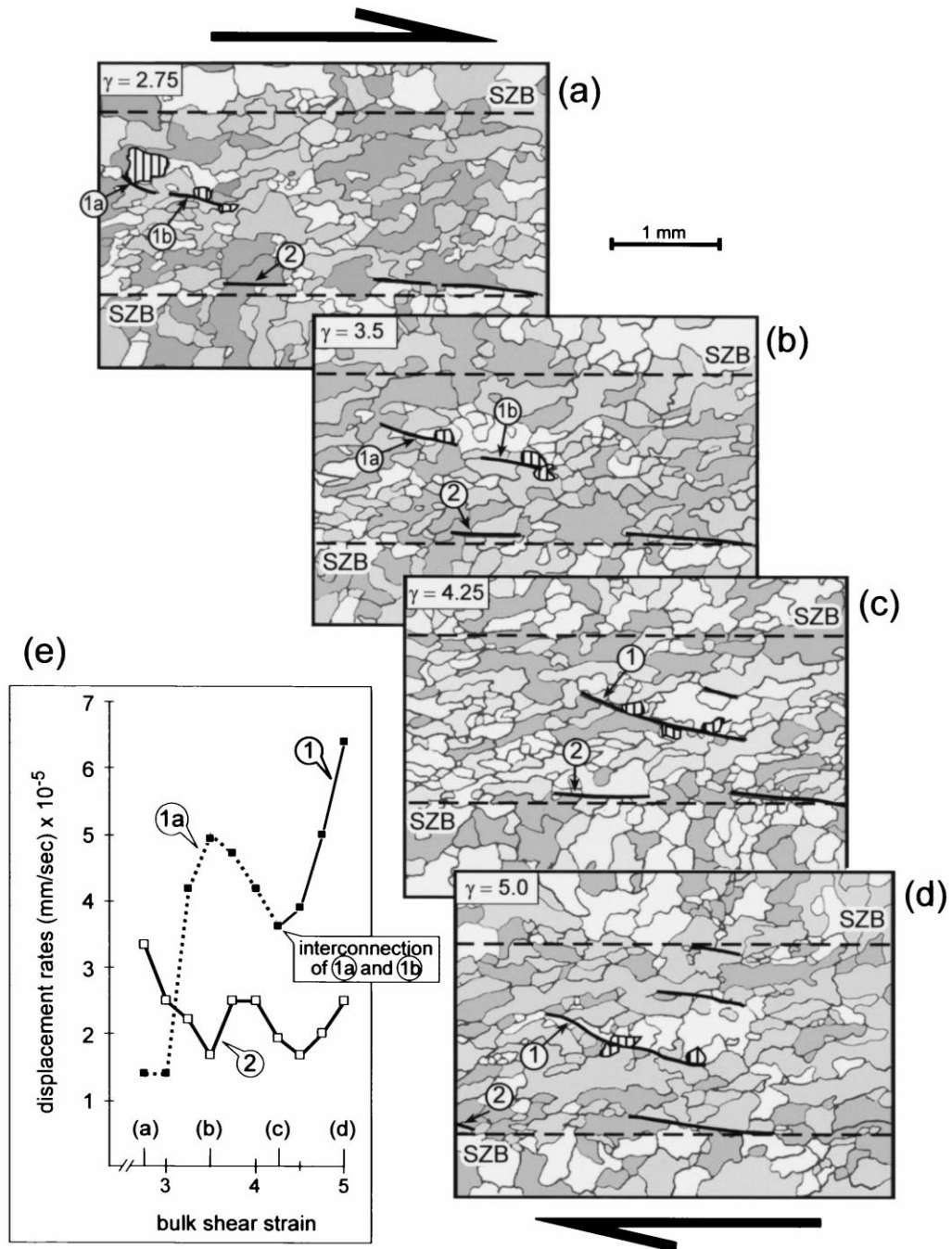


Fig. 9. Microstructural evolution in norcamphor during simple shearing. (a–d) Grain boundary drawings for four stages of deformation with propagating and interconnecting dilatant shear surfaces. Surfaces numbered 1a, 1b and 2 discussed in text. (e) Fluctuating displacement rate parallel to surfaces numbered 1a, 1 and 2 (see text for explanation). Vertically hatched grains serve as displacement markers. Changes in size and shape of these grains is due to syntectonic, grain boundary migration recrystallization. Experimental conditions: $T=25^{\circ}\text{C}$, $\dot{\gamma}=8.2 \times 10^{-5} \text{ s}^{-1}$.

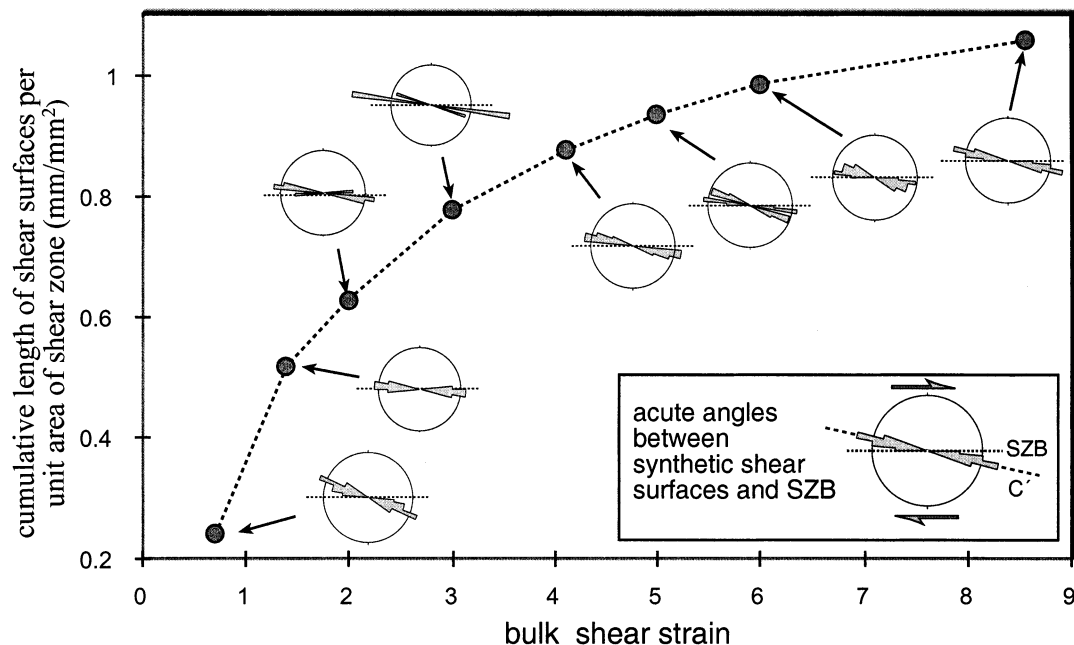


Fig. 10. Change in cumulative length of dilatant shear surfaces per unit area of shear zone versus shear strain. Solid circles indicate measurements. Rose diagrams indicate orientation of synthetic, dilatant shear surfaces with respect to the shear zone boundary. Experimental conditions: $T=10^{\circ}\text{C}$, $\dot{\gamma}=8 \times 10^{-5} \text{ s}^{-1}$.

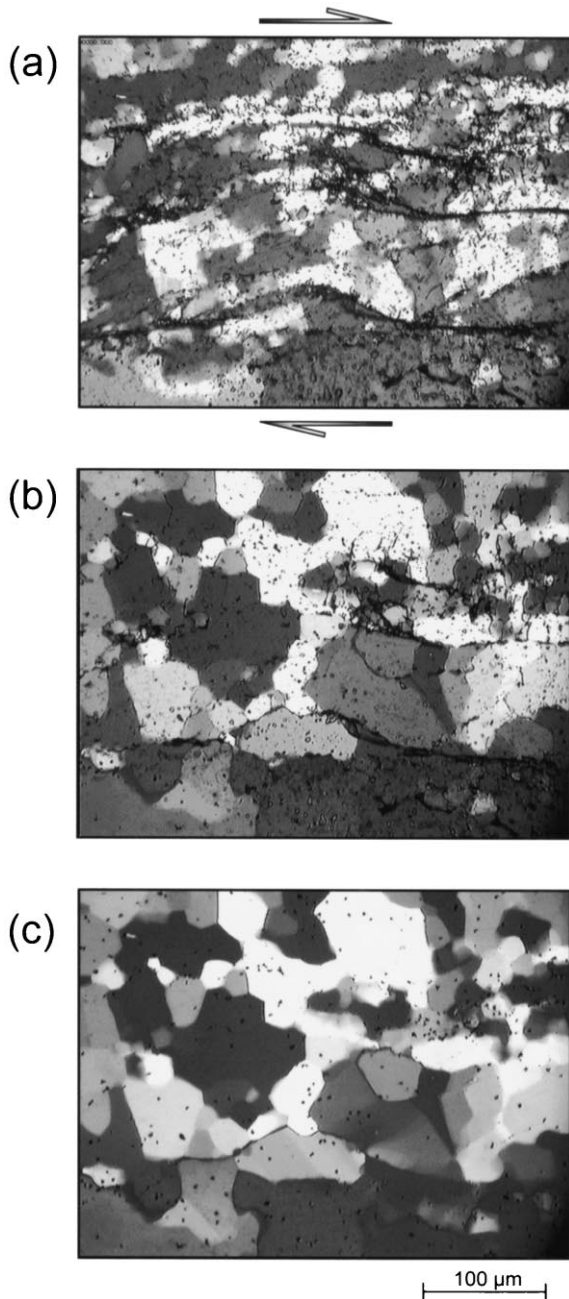
intracrystalline plasticity. Note that the displacement fluctuations for the dilatant shear surfaces are not always in phase with each other over the measured range of bulk shear strains. This indicates that the fluctuations are engendered locally within the deforming aggregate rather than by motor-induced variations in the ram speed.

The dilatant shear surfaces maintain a stable orientation at $\gamma > 2$, but on average, do not quite stop lengthening, even at a shear strain of $\gamma = 8.5$ (Fig. 10). The rose diagrams in Fig. 10 indicate that, following a slight antithetic rotation of about 10° at shear strains of $\gamma < 2$, the acute angle between the synthetic surfaces and the SZB remains constant at $10\text{--}15^{\circ}$. The nonlinear curve in Fig. 10 indicates that the dilatant shear surfaces lengthen more slowly with progressive shear strain. The steep slope of this curve to about $\gamma = 3$ is related to the rapid growth and coalescence of dilatant shear surfaces. The progressive shallowing of the curve at $\gamma \geq 3$ coincides with a gradual decrease in

the rate at which dilatant shear surfaces coalesce, coupled with more homogeneous deformation of the dynamically recrystallizing norcamphor matrix. The dilatant shear surfaces never interconnect completely to form a penetrative network that spans the entire experimental shear zone. Time-lapse video recordings of the evolving microstructure reveal that at the highest bulk shear strains ($\gamma = 7$ to 8.5), the few dilatant shear surfaces that appear to attain a steady-state length have a propagating tip at one end and a retreating tip at the other. Tip retreat occurs at compressional bridge structures between en échelon dilatant shear surfaces (Bauer et al., 2000).

The number of dilatant shear surfaces per unit area of sample (i.e. the areal density of shear surfaces) is also strongly dependent on temperature. Generally, fewer surfaces develop during deformation at higher experimental temperatures. This probably reflects the increased activity of dislocation creep (especially grain boundary migra-

tion recrystallization) and pressure solution, which act to relieve intergranular strain incompatibilities and so inhibit fracturing.

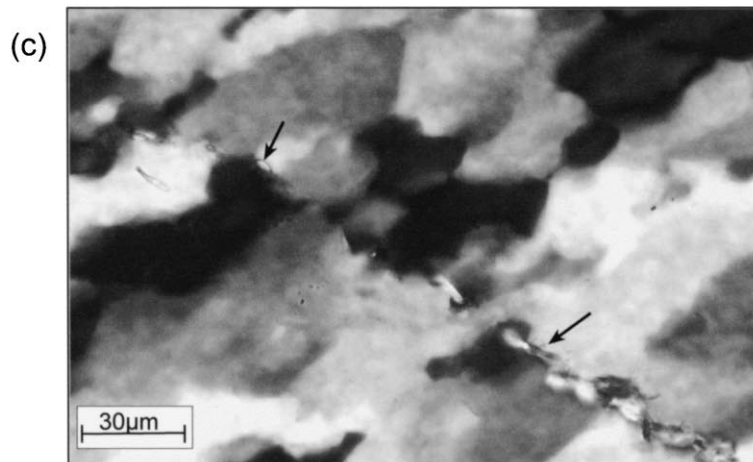
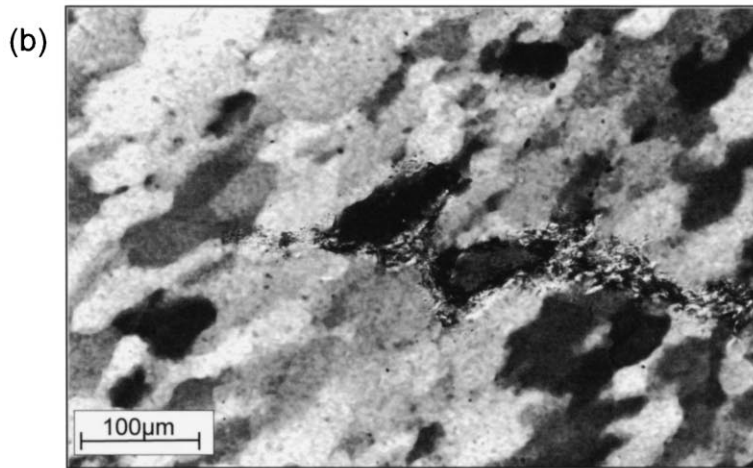
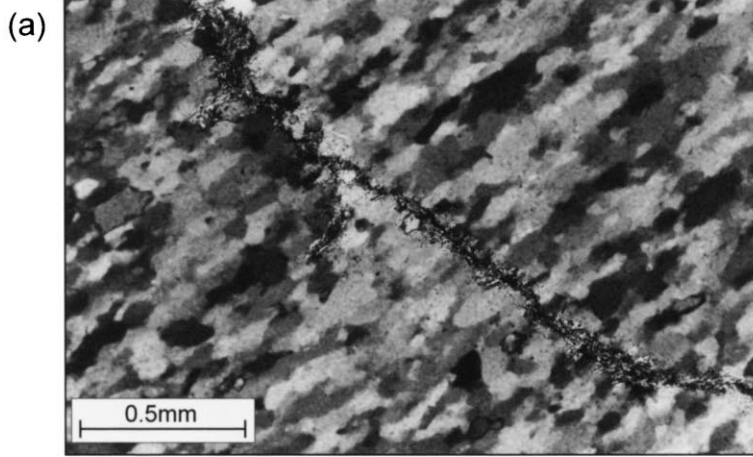


3.5. Effect of stress annealing

To determine the effect of post-tectonic annealing on the fluid-bearing shear surfaces in mylonitic norcamphor, we conducted an experiment in which the temperature of 20°C was maintained for 100 h after stopping the simple shear deformation (Fig. 11). The sample relaxed and, under the influence of the vertical stress field induced by the four screws holding down the metal covering plate, flattened and spread towards both of its ends (i.e. parallel to the frosted grips defining the SZB during simple shearing). Spreading of the sample was accompanied by progressive closure of the fluid-filled shear surfaces from the centre to the margins of the sample, causing most of the fluid to be squeezed to the edge of the sample. The norcamphor grains recrystallized to a larger size (600 µm) and acquired stable, equant grain shapes and boundaries (Fig. 11b). After prolonged stress annealing (Fig. 11c), the only visible remains of the dilatant shear surfaces are domains of locally smaller grains. Fluid pockets (tubules) remained at grain triple junctions and boundaries. Fluid inclusions, visible as black spots and trails in Fig. 11a, were swept by mobile grain boundaries during grain growth. Most of the black spots remaining in Fig. 11c are not fluid inclusions, but corundum marker particles used for strain analysis.

To summarize, the syntectonic distribution of fluid within polycrystalline norcamphor is closely related to pronounced strain localization along dilatant shear surfaces. These surfaces evolve during two successive stages: (1) the opening and interconnection of fluid-filled grain boundaries

Fig. 11. Stress annealing of a deformed norcamphor aggregate for 100 h at 20°C: (a) onset of stress annealing at the end of deformation; (b) after 50 h of stress annealing; (c) after 100 h of stress annealing. Note the progressive loss of dilatant, fluid-filled shear surfaces, and the coarsening and equilibration of the original dynamic microstructure. The black specks in (c) are corundum marker particles that remain visible after all fluid inclusions have disappeared during stress annealing. Photographs taken with crossed nichols. Scale same for all photographs. Experimental conditions prior to onset of stress annealing: $T = 20^\circ\text{C}$, $\dot{\gamma} = 8.6 \times 10^{-5} \text{ s}^{-1}$.



lead to the formation of dilatant shear surfaces oriented at low angles to the SZB; and (2) the episodic propagation and coalescence of these dilatant shear surfaces at low angles to the SZB. The propagation of the dilatant shear surfaces involves alternating intracrystalline plasticity and subcritical fracturing, concomitant with dynamic recrystallization and pressure solution in the rest of the sample. Because all shear surfaces are fluid-filled, their coalescence represents a strain-dependent increase in the interconnected porosity of the deforming norcamphor subparallel to the shear zone boundaries, as discussed below. Prolonged stress annealing decreases this porosity and removes most traces of the syntectonic fluid pathways.

4. Comparison of microstructures in norcamphor and deformed rocks

4.1. Fluid flow in dilatant fractures of dynamically recrystallized quartz

How relevant are our observations of deformation-induced fluid migration in norcamphor to the study of fluid pathways in naturally and experimentally deformed rocks? Although past studies have confirmed the resemblance of microfabrics in dry polycrystalline norcamphor and naturally deformed, metamorphic quartz (Herwegh and Handy, 1996, 1998; Herwegh et al., 1997), we pose this question again due to differences in the volume proportion of fluid in our norcamphor samples (10–15 vol% water) with that in natural metamorphic rocks, and to the contrasting solubilities of norcamphor and quartz in water discussed above (Fig. 3). Also, we were not sure whether the fluid redistribution mechanisms observed during simple shearing of wet norcamphor had counterparts in rocks deformed in general noncoaxial shear in nature, or in coaxial flattening in experiments. In

seeking evidence for related fracture- and fluid-flow processes in nature and experiment, we were aware that an organic compound like norcamphor cannot possibly behave like a rock in every respect.

Fig. 12 depicts the dynamically recrystallized quartz microstructure from a micaceous gneiss that underwent general, noncoaxial shear under retrograde, greenschist facies conditions (for details of the regional geology, see Handy, 1987). The length axes of the dynamically recrystallized quartz aggregates define an oblique SPO that leans in the dextral direction of shear (Fig. 12a). Fine white mica grains define an irregular surface that cuts across the dynamically recrystallized matrix and is oblique to the horizontal SZB (Fig. 12b). The attitude of this oblique surface with respect to the sense of shear in the dynamically recrystallized quartz matrix is diagnostic of a dilatant shear fracture that opened during dextral mylonitic shearing. Observed in detail, the white mica grains nucleate along quartz–quartz grain boundaries (Fig. 12b, arrows in Fig. 12c). White micas along the quartz–quartz grain boundaries also define the tips of the inferred fracture surface (Fig. 12b and c). Grain boundary migration recrystallization in quartz continued after the growth of white mica, as indicated by the curved quartz–quartz grain boundaries that transect the train of white mica grains (Fig. 12c). The lack of evidence for annealing of quartz (i.e. straight grain boundaries, uniform optical extinction of quartz) indicates that both temperature and differential stress dropped quickly at the end of deformation (Prior et al., 1990).

The white mica in Fig. 12 is interpreted to have precipitated from a metamorphic fluid that circulated along a dilatant fracture during retrograde, greenschist facies mylonitization. This fracture was oriented similarly with respect to the bulk shearing plane as the dilatant shear surfaces documented above in experimentally deformed, water-bearing norcamphor. The fluid must have left the fracture (and the rock?) during mylonitization, as evidenced

Fig. 12. Former dilatant surfaces in dynamically recrystallized quartz of a greenschist facies mylonite. (a) White mica aggregates mark remains of a fluid-filled fracture within dynamically recrystallized quartz. SPO in quartz indicates dextral sense of shear. (b) Tip of former fracture, marked by fine blades of white mica along the quartz grain boundaries. (c) Close-up of healed fracture marked by white mica grains (arrows) aligned oblique to the SPO in quartz. Shear zone boundary (SZB) is horizontal in all figures.

by the fact that grain boundary migration in quartz continued after the nucleation and growth of white mica. This behaviour contrasts with our wet norcamphor experiments, in which the water was constrained to remain in the samples during simple shearing at constant pore fluid pressure until the samples were subjected to prolonged stress annealing at constant temperature.

4.2. Comparison with experimentally deformed minerals

In comparing the microstructures of wet norcamphor with those of minerals that were experimentally deformed in the presence of a fluid phase, we found a number of striking similarities and differences:

(1) The opening at low strains of fluid-filled norcamphor grain boundaries oriented parallel to the principal compressive stress direction is similar to that observed in deformed polycrystalline agate containing 2–4% water (Karato and Masuda, 1989). Deformation-induced redistribution of fluid from tubules to grain faces is also observed in coaxially deformed, fine-grained polycrystalline feldspar with small quantities (0.7–0.8 wt%) of water (Tullis et al., 1996), although all feldspar grain boundaries (not just those oriented parallel to compression) dilated and deformation involved diffusion creep. In polycrystalline quartz with 2 wt% water (Tullis et al., 1996), however, the fluid remained in isolated pores and showed no tendency to migrate along open grain–grain faces during dynamic recrystallization. The relatively high fluid mobility in dynamically recrystallizing norcamphor probably reflects both the small water/norcamphor dihedral angle (ca. 46°) compared with that of water/quartz ($>60^\circ$; Laporte and Watson, 1991) and the isotropic interfacial energy characteristics of quartz (Tullis et al., 1996).

(2) In our experiments, wetted or fluid-filled norcamphor grain boundaries were not as mobile as dry grain boundaries. The retarded migration of wetted norcamphor grain boundaries contrasts with evidence for fluid-enhanced grain boundary mobility in experimentally deformed, hydrous feldspar aggregates (Tullis et al., 1996). This discrepancy may be due to the greater width of the fluid-

filled intergranular spaces in our experiments (ca. $30\ \mu\text{m}$ in norcamphor, $<1\ \mu\text{m}$ in the experimentally deformed feldspar of Tullis et al., 1996). Urai et al. (1986) proposed that greater fluid film thicknesses render intergranular diffusion (rather than dissolution or precipitation) of the solute the process that limits the migration rate of grain boundaries separated by fluid channels. They concluded that the rate of grain boundary migration is inversely proportional to the fluid film thickness, and invoked this relationship to interpret fluid inclusions along grain faces as relics of thicker, fluid-filled grain boundaries that had survived grain boundary migration recrystallization. The occurrence of similar fluid pockets and films along norcamphor grain boundaries in our experiments is consistent with this explanation.

(3) The greater activity in wet norcamphor of grain boundary migration recrystallization compared with subgrain-rotation recrystallization is also observed in mineral aggregates that were deformed at high homologous temperatures: calcite (Schmid et al., 1980); quartz (Hirth and Tullis, 1992); and sodium nitrate, a rock analogue for calcite (Tungatt and Humphreys, 1981).

The examples in this section confirm that the dilatant, fluid-filled surfaces similar to those observed in dynamically recrystallizing norcamphor also formed in natural quartz mylonites. These shear surfaces serve as fluid pathways and are easily overlooked in dynamically recrystallized minerals because microstructural traces of localized deformation and fluid flow other than the alignment of secondary, hydrous minerals are not always preserved (e.g. Beach, 1980; O'Hara, 1988), even if stress and temperature drops at the end of deformation were rapid. Irrespective of the differences between norcamphor and the minerals discussed above, the similar geometry of dilatant surfaces in dynamically recrystallizing norcamphor and metamorphic quartz warrants a discussion of how fluids and fractures in our experiments interact to create fluid pathways during mylonitization.

5. Discussion of the role of fluid during deformation

Clearly, the water in the norcamphor aggregates is at least partly responsible for the initial opening

and interconnection of grain boundaries oriented subparallel to the principal shortening direction (i.e. at about 45° to the SZB), because no such grain boundary dilation was observed in dry polycrystalline norcamphor subjected to simple shearing at similar temperatures and shear strain rates (Herwegh and Handy, 1996). It is therefore reasonable to interpret these fluid-filled, dilatational grain boundaries as hydrofractures, that is, as fractures that opened solely in response to reduced effective normal stress on grain boundaries. We note, however, that Ree (1994) also observed opening of grain boundaries oriented at low angles to the principal shortening direction during both pure and simple shearing of dry octachloropropane, another hexagonal organic, quartz analogue material. The open grain boundaries were filled with octachloropropane vapour, but never evolved into macroscopic fractures like the dilatant shear surfaces in our experiments. This indicates that a pressurized fluid may not be solely responsible for the geometry of the dilatant surfaces in our experiments on norcamphor. We therefore interpret the low strain, intergranular network of open surfaces generated at very low shear strains during the initial stage of our experiments to reflect a combination of two effects: (1) a grain boundary fluid at near-lithostatic pressure that acts to reduce the effective normal stress on grain boundaries (i.e. the law of effective stress, or Terzaghi's Law); and (2) grain boundaries that serve either as stress concentrators or as zones of pre-existing weakness. The positive feedback relationship between these effects (i.e. pre-existing zones of weakness dilate, draw pressurized fluid and become weaker in the presence of this fluid) localizes strain on the supra-granular scale.

The grain boundary fracturing observed at low strains in all of our experiments may correspond to cleavage 2 or 3 fracturing of Ashby et al. (1979), as recognized in rocks (Mitra, 1984; Wojtal and Mitra, 1986) and many crystalline materials undergoing crystal plastic deformation (e.g. metals and alloys; Ashby et al., 1979; Gandhi and Ashby, 1979). This type of intergranular fracturing involves the loss of grain–grain cohesion (also termed 'intercrystalline fracturing' by Cox and Etheridge, 1989) and relieves stress concentrations

that arise locally between grains when dynamic recrystallization is too slow and/or dislocation glide occurs on an insufficient number of independent slip systems for neighbouring grains in the aggregate to deform compatibly. Indeed, at the onset of deformation, the randomly distributed grain boundary fluid pockets themselves are mechanical heterogeneities that reduce the effective stress and facilitate intergranular fracturing. In experimentally deformed mineral aggregates, this type of fracturing is generally associated with subcritical crack velocities (Atkinson and Meridith, 1987), as also observed in our experiments.

The linkage of intergranular grain boundary openings to form transgranular dilatant shear surfaces represents a strain-dependent transition from primarily extensional (mode 1) fracturing to primarily shear (mode 2) fracturing towards the end of the initial stage of our experiments. With continued deformation, decelerating displacement along (i.e. parallel to) the dilatant shear surfaces is accommodated at their propagating tips primarily by dynamic recovery and dynamic recrystallization. Grains at these tips are inferred to harden, until the shear strength of norcamphor is exceeded and either intergranular or intragranular fractures develop, depending on the temperature (Fig. 4). The orientation of the crack tips is comparable with that of the host shear surface. Surface tip propagation by intergranular and intragranular fracturing at high and low temperatures, respectively, is consistent with temperature-dependent differences of fracture mechanisms observed in a wide variety of hexagonal metals and alloys (Gandhi and Ashby, 1979).

In contrast to the mechanical effects outlined above, the chemical role of the fluid during our experiments is not as well constrained. The occurrence of pressure solution in our experiments certainly reflects the high solubility of norcamphor in water at room temperature and pressure (recall Fig. 3). Pressure solution is most evident at low strains and effects the transfer of norcamphor from locally stressed sites to dilating, fluid-filled spaces (e.g. incipient, dilatant shear surfaces, Fig. 5). At high shear strains, particularly adjacent to the dilatant shear surfaces, the rates of dissolution,

diffusion and/or precipitation of norcamphor in water appear to be too low to accommodate the imposed strain compatibly by pressure solution alone. Thermally activated dislocation creep (involving both grain boundary migration and subgrain-rotation recrystallization) and fracturing were thus the dominant deformation mechanisms in our experiments.

The fluid therefore appears to have played a dual role during deformation. By enhancing fracturing and enabling pressure solution, the fluid contributed to the rapid creation of interconnected porosity at sites of stress concentration and/or pre-existing weakness. By filling and sealing dilational volumes, however, the fluid also contributed to the local destruction of connected pore space. At low strains, the rate at which interconnected porosity was created exceeded that at which it was destroyed. At high shear strains, however, most of the fluid was segregated into the dilatant shear surfaces, limiting the fluid's mechanical–chemical influence to the immediate vicinity of these surfaces. In the norcamphor matrix between the fluid-filled shear surfaces, grain boundary mobility was enhanced by the absence of thick fluid films and deformation became more homogeneous. Thus, a balance between the rates of pore connectivity creation and destruction was achieved. The attainment of this balance is reflected in the flattening of the cumulative shear surface length/unit area versus shear strain curve in Fig. 10.

6. Implications for fluid mobility in mylonitic shear zones

The strain-dependent changes in microstructure and fluid distribution in norcamphor have important implications, both for the evolution of fluid pathways in the continental crust, and for the permeability of crustal rocks at the brittle to viscous transition. We emphasize, however, that fluid migration and deformation involve inter-related processes which, given the current limits of modelling with rock analogues, were at best simulated qualitatively in our experiments.

In general, the two variables that most influence fluid mobility in rocks are permeability and the

hydraulic head gradient. According to Darcy's Law, increased permeability and supra-hydrostatic fluid pressure gradients increase the advective flux of pore fluid of a given density and kinematic viscosity. Permeability is in turn primarily a nonlinear function of porosity and the geometry of the pore space (e.g. Thompson and Connolly, 1990 and references cited therein). If the porosity is too small, then fluid flow may slow or even cease because interactions between the fluid and the walls of very narrow capillary spaces (e.g. grain boundary tubules) can retard flow significantly. This may pertain to the initial (i.e. pre-deformational) norcamphor microstructure in our experiments. Our experiments show that, even at constant, high pore fluid pressure, in the absence of deformation the fluid is initially restricted to intergranular pockets and tubules between norcamphor grains. The permeability of this microstructure is expected to be relatively low. With the onset of deformation, fluid migrates to dilational grain boundaries and is then channelled along elongate, dilatant shear surfaces at low angles to the shearing plane. Modelling studies have demonstrated that fluid advection in media with open surfaces is enhanced relative to those with narrow, interconnected tubules, even when the surfaces are uneven (Brown et al., 1998). Moreover, experiments on mineral aggregates at controlled effective pressure, temperature and strain rate have shown that the strain-dependent connection of pore space can increase rock permeability by several orders of magnitude, especially at high pore fluid pressures (Fischer and Paterson, 1992; Zhang et al., 1994).

We recall that high pore fluid pressure is a partial requisite for the nucleation and growth of the dilatant shear surfaces from fluid-filled grain boundaries. Thus, shear zones active in high fluid pressure regimes as simulated in our experiments will preferentially develop such structures. Because the dilatant shear surfaces are oriented at low angles to the mylonitic foliation and SZB, both porosity and permeability within the shear zone are expected to be highly anisotropic, with fluid migrating parallel to subparallel to the shearing plane, as documented in several field studies (e.g. McCaig, 1987; Marquer and Burkhard, 1992). A

point worth re-iterating in this context, however, is that the dilatant shear surfaces in norcamphor are never completely and simultaneously interconnected along the length of the entire shear zone. Thus, fluid flux along the shear zone in the direction of shear is probably limited by the rate at which the tips of the dilatant shear surfaces propagate subparallel to the shearing plane.

Anisotropic porosity and permeability are also expected to be characteristic of mylonitic shear zones with more general, three-dimensional bulk strain configurations than the two-dimensional configuration of our simple shear experiments. A greater component of coaxial deformation produces mylonitic shear zones at high angles and varied orientations to the principal shortening direction (Gapais et al., 1987). This would increase pore connectivity within the plane of shear in directions oblique to the bulk shearing direction. Because our experiments on wet norcamphor were undrained, there were obviously no sample-scale, fluid pressure gradients during shearing. Strictly speaking, our experiments therefore simulate closed system behaviour. However, we have performed partly drained, simple shear experiments on partially melted norcamphor–benzamide aggregates and found that melts are sucked into dilatant shear surfaces and exit the sample rapidly down melt pressure gradients along these shear surfaces (Rosenberg and Handy, 1997, 2000). Migration of overpressurized melt parallel to mylonitic foliation but oblique to the shearing direction was inferred from a geometric analysis of synmylonitic mafic veins in an upper amphibolite facies shear zone that accommodated general noncoaxial shear (Handy and Streit, 1999). Taken together, the evidence above suggests that the fluid-flow direction in shear zones that are open to fluid flow is not only affected by the kinematics of deformation (noncoaxial versus coaxial shear), but also by the direction and magnitude of the syntectonic fluid pressure gradient with respect to the orientation of the mylonitic foliation and the plane of shear. This might explain the general lack of a consistent relationship between the kinematics of shearing and the direction of fluid flow inferred from isotopic studies of syntectonic vein minerals within

several large-scale shear zones (e.g. Streit and Cox, 1998 and references cited therein).

7. Summary

Polycrystalline norcamphor mixed with 10–15 vol% water and subjected to simple shearing has proved to be a good analogue for simulating fluid flow in dynamically recrystallizing quartz at high pore fluid pressure. Fig. 13 summarizes the strain localization and fluid distribution relations inferred from this study and illustrates some new and modified notions on fluid flow patterns in deep crustal mylonite. The pore connectivity versus bulk shear strain curve in Fig. 13 is derived from the cumulative shear surface length versus strain curve in Fig. 10, indicating strain-dependent changes in the fluid distribution during dynamic recrystallization of norcamphor (boxes at bottom of Fig. 13). We use this approach to infer the evolution of pore connectivity subparallel to mylonitic foliation in a quartz-rich rock deforming aseismically at constant, near-lithostatic pore fluid pressure ($\lambda_v \approx 1$).

At very low strains, pore connectivity is low (stage I in Fig. 13). After only small shear strains, however, pore connectivity increases dramatically due to the coalescence of fluid-filled grain boundaries to form dilatant shear surfaces (stage II in Fig. 13). The formation of dilatant shear surfaces represents the attainment of a first percolation threshold subparallel to the shearing plane. At intermediate to high shear strains, pore connectivity increases more gradually with strain (stage III Fig. 13), reflecting the almost complete segregation of fluid into dilatant shear surfaces and a balance of processes that create interconnected pore space (hydrofracturing, dissolution) and processes that destroy this connectivity (dynamic recrystallization, solute precipitation), as observed in wet norcamphor. Fluid flow is focused along dilatant, fluid-filled shear surfaces that propagate alternately by intracrystalline plasticity and subcritical hydrofracturing, while the rest of the sample that has been swept of most fluids undergoes dynamic recrystallization. For a given fluid pressure gradient parallel to the shearing

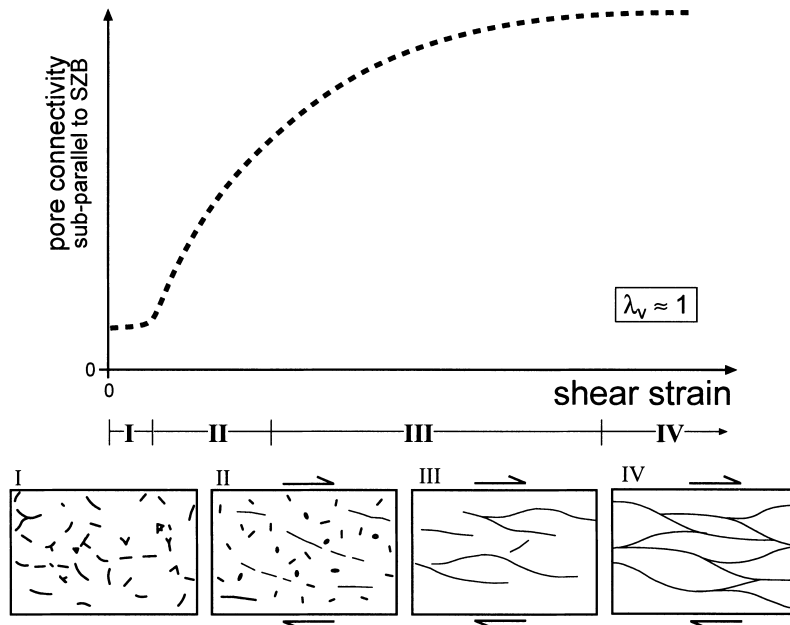


Fig. 13. Summary of changes in interconnected porosity as a function of shear strain, as inferred from this study at constant pore fluid pressure (P_p), strain rate and temperature. Four boxes show strain-dependent change in grain-scale fluid distribution (fluid sites depicted schematically as dots and lines) for the porosity evolution described in the text (stages I to IV).

plane, permeability along the mylonitic foliation during stage III is expected to scale nonlinearly with the length, connectivity and propagation rate of dilatant shear surfaces.

If the rates of creating and destroying pore connectivity are equal, then the interconnected porosity never evolves beyond that shown in stage III of Fig. 13, even at high strains and in the presence of fluid at lithostatic pore fluid pressure. This pertains to mylonites deforming at conditions (high homologous temperatures and/or low strain rates) favouring processes (rapid grain boundary migration and/or pressure solution) which destroy connective porosity and suppress critical fracture propagation. However, transient fluctuations in pore fluid pressure from subhydrostatic to supralithostatic levels in mylonite deforming at low homologous temperatures and/or high strain rates may enhance critical fracture propagation and favour the development of an interconnected fluid-flow network or 'backbone' porosity along discrete high-strain zones (stage IV in Fig. 13). The establishment of a flow backbone represents a second percolation threshold at higher strains than the

first threshold above, and is probably associated with a marked increase in permeability (Cox, 1999). However, we were unable to simulate a flow backbone under a hydraulic head gradient in our experiments. We expect large, short-term fluctuations in pore fluid pressure along a flow backbone to be more common in mylonites undergoing fault valve behaviour at the seismic–aseismic transition zone in the crust (e.g. Cox, 1995) or in fault rocks within the seismogenic regime where cataclasis is the dominant deformation mechanism (e.g. Matthai and Fischer, 1996; Sibson, 1996).

To our knowledge, there are currently no quantitative, theoretical models of shear zone nucleation and propagation which account for the interaction of subcritical fracturing, fluid flow, dynamic recrystallization and pressure solution observed in our experiments. Rutter and Brodie's (1985) model of hydrous shear zone propagation controlled by fluid permeation is an attractive start, but requires modification to account for dilatancy associated with fracturing.

Our in situ study of polycrystalline norcamphor mixed with water is certainly not exhaustive in its

investigation of fluid pathways during strain localization. Future work with analogue materials should be directed at simulating syntectonic metamorphic reactions that involve a fluid phase, as such reactions probably affect the hydrogeology of shear zones and hence also the local rheology. In addition, fluid flow is linked to dilatant processes (e.g. opening of grain boundaries, fracturing) that are dependent on effective pressure. In situ experiments at controlled confining pressure (Bauer et al., 2000) and pore fluid pressure will yield potentially valuable insight into such processes.

Acknowledgements

Our sincere thanks go to Jürgen Streit who began this work with us in 1995 before moving to ANU in the summer of 1997. During this time and after, he discussed many aspects of our research with us. Marco Herwegh and Bas den Brok helped introduce one of us (P.B.) to rock analogue materials. Claudio Rosenberg was a constant source of inspiration in the laboratory. This paper benefitted from the constructive reviews of Ernie Rutter and Rudi Wenk, as well as from the helpful comments of Jan Tullis, Win Means and Jürgen Streit. Paul Bons made some useful suggestions regarding semantics and the visual presentation of our data. Finally, we thank Jochen Babist for last-minute help with drafting the figures. This work was supported by the German Science Foundation (DFG) in the form of Project Grant Ha 2403/1.

References

- Ashby, M.F., Ghandi, C., Taplin, D.M.R., 1979. Fracture mechanism maps and their construction for fcc metals and alloys, overview no. 3. *Acta Metall.* 27, 699–729.
- Atkinson, B.K., Meridith, P.G., 1987. The theory of subcritical crack growth with applications to minerals and rocks. In: Atkinson, K. (Ed.), *Fracture Mechanics of Rock*. Academic Press, London, pp. 111–166.
- Bauer, P., Rosenberg, C.L., Handy, M.R., 2000. Deformation experiments on rock analogue materials at controlled confining pressure: a new approach for studying strain localization at the brittle to viscous transition. *J. Struct. Geol.* 22 (3), 281–289.
- Beach, A., 1980. Retrograde metamorphic processes in shear zones with special reference to the Lewisian complex. *J. Struct. Geol.* 2, 257–263.
- Bell, T.H., Hayward, N., 1991. Episodic metamorphic reactions during orogenesis: the control of deformation partitioning on reaction sites and reaction duration. *J. Metamorph. Geol.* 9, 619–640.
- Blanpied, M.L., Lockner, D.A., Byerlee, J.D., 1992. An earthquake mechanism based on rapid sealing of faults. *Nature* 358, 574–575.
- Bons, P.D., 1993. Experimental deformation of polyphase rock analogues. *Geol. Ultraject.* 110, 1–207.
- Bons, P.D., Jessel, M.W., Passchier, C.W., 1993. The analysis of progressive deformation in rock analogues. *J. Struct. Geol.* 15, 3–5, 403–412.
- Brodie, K.H., Rutter, E.H., 1985. On the relationship between deformation and metamorphism with special reference to the behaviour of basic rocks. In: Thompson, A.B., Rubie, D.C. (Eds.), *Metamorphic Reactions: Kinetics, Textures, and Deformation. Advances in Physical Geochemistry Vol. 4*. Springer, New York, pp. 138–179.
- Brodie, K.H., Rutter, E.H., 1987. The role of transiently fine grained reaction products in syntectonic metamorphism. *Can. J. Earth Sci.* 24, 556–564.
- Brown, S., Caprihan, A., Hardy, R., 1998. Experimental observation of fluid flow channels in a single fracture. *J. Geophys. Res.* 103, B3, 5125–5132.
- Cox, S.F., 1995. Faulting processes at high fluid pressures: an example of fault valve behaviour from the Wattle Gully Fault, Victoria. *J. Geophys. Res.* 100, 841–859.
- Cox, S.F., 1999. Deformation controls on the dynamics of fluid flow in mesothermal gold systems. In: McCaffrey, K.J.W., Lonergan, L., Wilkinson, J.J. (Eds.), *Fractures, Fluid Flow and Mineralization*, *Geol. Soc. London Spec. Publ.* 155, 123–140.
- Cox, S.F., Etheridge, M.A., 1989. Coupled grain-scale dilatancy and mass transfer during deformation at high fluid pressures: examples from Mount Lyell, Tasmania. *J. Struct. Geol.* 11 (1), 147–162.
- Drury, M.R., Urai, J.L., 1990. Deformation-related recrystallization processes. *Tectonophysics* 172, 235–253.
- Dutrage, G., Burg, J.P., 1998. Strain localization in an orthogneiss laccolith (the Pinet Massif, Aveyron, southern France). *Tectonophysics* 280, 1/2, 47–60.
- Etheridge, M.A., Wall, V.T., Vernon, R.H., 1983. The role of the fluid phase during regional metamorphism and deformation. *J. Metamorph. Geol.* 1 (3), 205–226.
- Etheridge, M.A., Wall, V.T., Cox, S.F., 1984. High fluid pressures during regional metamorphism and deformation: implications for mass transport and deformation mechanisms. *J. Geophys. Res.* 89 (36), 4344–4358.
- Etheridge, M.A., Symonds, P.A., Powell, T.G., 1988. Application of the detachment model for continental extension to hydrocarbon exploration in extensional basins. *APEA J.*, 167–187.

- Fischer, G.J., Paterson, M.S., 1992. Measurements of permeability and storage capacity in rocks during deformation at high temperature and pressure. In: Evans, B., Wong, T.-F. (Eds.), *Fault Mechanics and Transport Properties of Rocks*. Academic Press, San Diego, pp. 213–252.
- Fricke, H.C., Wickham, S.M., O'Neil, J.R., 1992. Oxygen and hydrogen isotope evidence for meteoric water infiltration during mylonitization and uplift in the Ruby Mountains–East Humboldt Range core complex, Nevada. *Contrib. Mineral. Petrol.* 111, 203–221.
- Gandhi, C., Ashby, M.F., 1979. Fracture mechanism maps for materials which cleave: fcc, bcc and hcp metals and ceramics, overview no. 5. *Acta Metall.* 27, 1565–1602.
- Gapais, D., Bale, P., Choukroune, P., Cobbold, P.R., Mahjoub, Y., Marquer, D., 1987. Bulk kinematics from shear zone patterns: Some field examples. *J. Struct. Geol.* 9, (5/6), 635–646.
- Handin, J., Hager Jr., R.V., Friedman, M., Feather, J.N., 1963. Experimental deformation of sedimentary rocks under confining pressure: pore pressure tests. *Am. Assoc. Petrol. Geol. Bull.* 47, 718–755.
- Handy, M.R., 1987. The structure, age and kinematics of the Pogallo fault zone, Southern Alps, northwestern Italy. *Ecol. geol. Helv.* 80 (3), 593–632.
- Handy, M.R., Streit, J.E., 1999. Mechanisms and mechanics of magmatic underplating: inferences from syntectonic mafic veins in deep crustal mylonite. *Earth Planet. Sci. Lett.* 165, 271–286.
- Heard, H.C., Rubey, W.W., 1966. Tectonic implications of gypsum dehydration. *Geol. Soc. Am. Bull.* 77, 741–760.
- Herwegh, M., Handy, M.R., 1996. The evolution of high temperature mylonitic microfibrils: evidence from simple shearing of a quartz analogue (norcamphor). *J. Struct. Geol.* 18 (5), 689–710.
- Herwegh, M., Handy, M.R., 1998. The origin of shape preferred orientations in mylonite: inferences from in situ experiments on polycrystalline norcamphor. *J. Struct. Geol.* 20 (6), 681–694.
- Herwegh, M., Handy, M.R., Heilbronner-Panozzo, R., 1997. Temperature and strain rate dependent microfabric evolution in monomineralic mylonite: evidence from in situ deformation of a rock analogue. *Tectonophysics* 280, 1/2, 83–106.
- Hirth, G., Tullis, J., 1992. Dislocation creep regimes in quartz aggregates. *J. Struct. Geol.* 14 (2), 145–160.
- Holness, M.B., 1997. The permeability of non-deforming rock. In: Holness, B. (Ed.), *Deformation-enhanced Fluid Transport in the Earth's Crust and Mantle*. The Mineralogical Society Series 8. Chapman and Hall, London, pp. 9–34.
- Jaoul, O., Tullis, J., Kronenberg, A.K., 1984. The effect of varying water contents on the creep behaviour of Heavitree Quartzite. *J. Geophys. Res.* 89, B6, 4281–4287.
- Karato, S., Masuda, T., 1989. Anisotropic grain growth in quartz aggregates under stress and its implication for foliation development. *Geology* 17, 695–698.
- Laporte, D., Watson, E.B., 1991. Direct observation of near-equilibrium pore geometry in synthetic crustal quartzites at 600–800°C and 2–10.5 kbars. *J. Geol.* 99, 873–878.
- Logan, J.M., Dengo, C., Higgs, M., Wang, Z.Z., 1992. Fabrics of experimental fault zones: their development and relationship to mechanical behavior. In: *Fault Mechanics and Transport Properties of Rock*. Academic Press, New York, pp. 34–67.
- Marquer, D., Burkhard, M., 1992. Fluid circulation, progressive deformation and mass-transfer processes in the upper crust: the example of basement-cover relationships in the External Crystalline Massifs, Switzerland. *J. Struct. Geol.* 14, 8/9, 1047–1057.
- Matthai, S.K., Fischer, G., 1996. Quantitative modelling of fault-fluid-discharge and fault-dilation induced fluid-pressure variations in the seismogenic regime. *Geology* 24, 183–186.
- McCaig, A., 1987. Deformation and fluid–rock interaction in metasomatic dilatant shear bands. *Tectonophysics* 135, 121–132.
- McCaig, A., Wickham, S.W., Taylor, H.P., 1990. Deep fluid circulation in alpine shear zones, Pyrenees, France: field and oxygen isotope studies. *Contrib. Miner. Petrol.* 106, 41–60.
- Means, W.D., 1977. A deformation experiment in transmitted light. *Earth Planet. Sci. Lett.* 35, 169–179.
- Means, W.D., 1989. Synkinematic microscopy of transparent polycrystals. *J. Struct. Geol.* 11, 1/2, 163–174.
- Mitra, G., 1984. Brittle to ductile transition due to large strains along the White Rock thrust, Wind River mountains, Wyoming. *J. Struct. Geol.* 6, 1/2, 51–61.
- Murrell, S.A.F., 1965. The effect of triaxial stress systems on the strength of rocks at atmospheric temperatures. *J. Roy. Astron. Soc.* 10, 231–281.
- Newton, R.C., 1990. Fluids and shear zones in the deep crust. *Tectonophysics* 182, 21–37.
- O'Hara, K., 1988. Fluid flow and volume loss during mylonitization: an origin for phyllonite in an overthrust setting, North Carolina, USA. *Tectonophysics* 156, 21–36.
- Petit, J.P., 1987. Criteria for movement on fault surfaces. *J. Struct. Geol.* 9, 5/6, 597–608.
- Platt, J.P., Vissers, R.L.M., 1980. Extensional structures in anisotropic rocks. *J. Struct. Geol.* 2 (4), 397–410.
- Prior, D.J., Knipe, R.J., Handy, M.R., 1990. Estimates of the rates of microstructural change in mylonites. In: Knipe, R.J., Rutter, E.H. (Eds.), *Deformation Mechanisms, Rheology and Tectonics*. *Geol. Soc. Spec. Publ.* 54, 309–320.
- Raleigh, C.B., Paterson, M.S., 1965. Experimental deformation of serpentinite and its tectonic implications. *J. Geophys. Res.* 70, 3965–3985.
- Ree, J.H., 1994. Grain boundary sliding and development of grain boundary openings in experimentally deformed octachloropropane. *J. Struct. Geol.* 16 (3), 403–418.
- Rosenberg, C.L., Handy, M.R., 1997. Synkinematic melt migration in a norcamphor/benzamide rock analogue. *Terra Abstr.* 9 (1), 456.
- Rosenberg, C.L., Handy, M.R., 2000. Syntectonic melt pathways during simple shearing of an anatectic rock analogue (norcamphor–benzamide). *J. Geophys. Res.* 105, 3135–3149.
- Rutter, E.H., 1972. The influence of interstitial water on the

- rheological behaviour of calcite rocks. *Tectonophysics* 14, 13–33.
- Rutter, E.H., 1983. Pressure solution in nature, theory and experiment. *J. Geol. Soc.* 140 (5), 725–740.
- Rutter, E.H., Brodie, K.H., 1985. The permeation of water into hydrating shear zones. In: Thompson, A.B., Rubie, D.C. (Eds.), *Metamorphic Reactions: Kinetics, Textures, and Deformation*. *Advances in Physical Geochemistry* Vol. 4. Springer, New York, pp. 242–250.
- Schmid, S.M., Handy, M.R., 1991. Towards a genetic classification of fault rocks: Geological usage and tectonophysical implications. In: Hsü, K.J., Mackenzie, J., Müller, D. (Eds.), *Controversies in Modern Geology*. Academic Press, London, pp. 339–361.
- Schmid, S.M., Paterson, M.S., Boland, J.N., 1980. High temperature flow and dynamic recrystallization in Carrara Marble. *Tectonophysics* 65, 3/4, 245–280.
- Selverstone, J., Morteani, G., Staude, J.-M., 1991. Fluid channelling during ductile shearing: transformation of granodiorite into aluminous schist in the Tauern Window, Eastern Alps. *J. Metamorph. Geol.* 9, 419–431.
- Shimamoto, T., 1989. The origin of S–C mylonites and a new fault-zone model. *J. Struct. Geol.* 11, 1/2, 51–64.
- Sibson, R.H., 1996. Structural permeability of fluid-driven fault-fracture meshes. *J. Struct. Geol.* 18, 1031–1042.
- Sibson, R.H., Moore, J.McM., Rankin, A.H., 1975. Seismic pumping — a hydrothermal fluid transport mechanism. *J. Geol. Soc. London* 131, 653–659.
- Streit, J.E., Cox, S.F., 1998. Fluid infiltration and volume change during mid-crustal mylonitization of Proterozoic granite, King Island, Tasmania. *J. Metamorph. Geol.* 16, 197–212.
- Thompson, A.B., Connolly, J.A.D., 1990. Metamorphic fluids and anomalous porosities in the lower crust. *Tectonophysics* 182, 47–55.
- Tullis, J., Yund, R., Farver, J., 1996. Deformation-enhanced fluid distribution in feldspar aggregates and implications for ductile shear zones. *Geology* 24 (1), 63–66.
- Tungatt, P.D., Humphreys, F.J., 1981. An in situ optical investigation of the deformation behavior of sodium nitrate — an analogue for calcite. *Tectonophysics* 78, 1–4, 661–676.
- Urai, J.L., 1983. Water-assisted dynamic recrystallization and weakening in polycrystalline bischofite. *Tectonophysics* 96, 125–157.
- Urai, J.L., Humphreys, F.J., Burrows, S.E., 1980. In situ studies of the deformation and dynamic recrystallization of rhombohedral camphor. *J. Mater. Sci.* 15, 1231–1240.
- Urai, J.L., Means, W.D., Lister, G.S., 1986. Dynamic recrystallization of minerals. In: Hobbs, B. E., Heard, H. C. (Eds.), *Mineral and Rock Deformation: Laboratory Studies — The Paterson Volume*, Am. Geophys. Union, Geophys. Monogr. 36, 161–199.
- Weijermars, R., 1986. Flow behaviour and physical chemistry of bouncing putties and related polymers in view of tectonic laboratory applications. *Tectonophysics* 124, 325–358.
- Wojtal, S., Mitra, G., 1986. Strain hardening and strain softening in fault zones from foreland thrusts. *Geol. Soc. Am. Bull.* 97, 674–687.
- Zhang, S., Cox, S.F., Paterson, M.S., 1994. The influence of room temperature deformation on porosity and permeability in calcite aggregates. *J. Geophys. Res.* 99, 15761–15775.